Real-time imaging reveals distinct pore scale dynamics during transient and equilibrium subsurface multiphase flow

Catherine Spurin[1], Tom Bultreys[2], Maja Ruecker[1], Gaetano Garfi[1], Christian M Schlepütz[3], Vladimir Novak[3], Steffen Berg[4], Martin Julian Blunt[5], and Samuel Krevor[1]

[1]Imperial College London
[2]Ghent University
[3]Paul Scherrer Institut
[4]Shell Global Solutions International B.V.
[5]Imperial College

November 26, 2022

Abstract

Many subsurface fluid flows, including the storage of CO underground or the production of oil, are transient processes incorporating multiple fluid phases. The fluids are not in equilibrium meaning macroscopic properties such as fluid saturation and pressure vary in space and time. However, these flows are traditionally modelled with equilibrium (or steady-state) flow properties, under the assumption that the pore scale fluid dynamics are equivalent. In this work, we used fast synchrotron X-ray tomography with 1s time resolution to image the pore scale fluid dynamics as the macroscopic flow transitioned to steady-state. For nitrogen or decane, and brine injected simultaneously into a porous rock we observed distinct pore scale fluid dynamics during transient flow. Transient flow was found to be characterised by intermittent fluid occupancy, whereby flow pathways through the pore space were constantly rearranging. The intermittent fluid occupancy was largest and most frequent when a fluid initially invaded the rock. But as the fluids established an equilibrium the dynamics decreased to either static interfaces between the fluids or small-scale intermittent flow pathways, depending on the capillary number and viscosity ratio. If the fluids were perturbed after an equilibrium was established, by changing the flow rate, the transition to a new equilibrium was quicker than the initial transition. Our observations suggest that transient flows require separate modelling parameters. The timescales required to achieve equilibrium suggest that several metres of an invading plume front will have flow properties controlled by transient pore scale fluid dynamics.

Real-time imaging reveals distinct pore scale dynamics during transient and equilibrium subsurface multiphase flow

Catherine Spurin[1], Tom Bultreys[1,3], Maja Rücker[2], Gaetano Garfi [1], Christian M. Schlepütz[4], Vladimir Novak[4], Steffen Berg[5], Martin J. Blunt[1]& Samuel Krevor[1]

[1]Department of Earth Science & Engineering, Imperial College London, UK
[2]Department of Chemical Engineering, Imperial College London, UK
[3]UGCT - PProGRess, Department of Geology, Ghent University, BE
[4]Swiss Light Source, Paul Scherrer Institute, CH
[5]Shell Global Solutions International B.V., NL

Key Points:

- We use synchrotron X-ray imaging to quantify the change in flow dynamics as the system transitions to steady-state.
- We observed distinct dynamics during transient flow which would suggest that transient flow should be modelled with separate parameters.
- We quantify the timescales for steady-state to be established for different capillary numbers and viscosity ratios.

Corresponding author: Catherine Spurin, `cls13@ic.ac.uk`

Abstract

Many subsurface fluid flows, including the storage of CO_2 underground or the production of oil, are transient processes incorporating multiple fluid phases. The fluids are not in equilibrium meaning macroscopic properties such as fluid saturation and pressure vary in space and time. However, these flows are traditionally modelled with equilibrium (or steady-state) flow properties, under the assumption that the pore scale fluid dynamics are equivalent. In this work, we used fast synchrotron X-ray tomography with $1s$ time resolution to image the pore scale fluid dynamics as the macroscopic flow transitioned to steady-state. For nitrogen or decane, and brine injected simultaneously into a porous rock we observed distinct pore scale fluid dynamics during transient flow. Transient flow was found to be characterised by intermittent fluid occupancy, whereby flow pathways through the pore space were constantly rearranging. The intermittent fluid occupancy was largest and most frequent when a fluid initially invaded the rock. But as the fluids established an equilibrium the dynamics decreased to either static interfaces between the fluids or small-scale intermittent flow pathways, depending on the capillary number and viscosity ratio. If the fluids were perturbed after an equilibrium was established, by changing the flow rate, the transition to a new equilibrium was quicker than the initial transition. Our observations suggest that transient flows require separate modelling parameters. The timescales required to achieve equilibrium suggest that several metres of an invading plume front will have flow properties controlled by transient pore scale fluid dynamics.

1 Introduction

Understanding the simultaneous flow of multiple fluids through the Earth's crust is a fundamental problem to our society. How fluids propagate, and become trapped, governs how safely CO_2 can be stored underground in saline aquifers to mitigate climate change (Rubin & De Coninck, 2005; Bachu, 2000; Bickle, 2009), if underground drinking water supplies will be protected from spilled non-aqueous contaminants (Pye & Patrick, 1983) and how much hydrocarbons will be produced from a reservoir (Blunt, 2017). The invasion of CO_2, or the contaminant, is a transient process; macroscopic fluid properties such as saturation and pressure vary in time and space. Under steady-state conditions, the fluids have established an equilibrium and macroscopic fluid properties are invariant in space (Tallakstad, Knudsen, et al., 2009). However, the prevailing theory of subsurface multiphase flows depends on the equivalency of underlying pore scale fluid dynamics during transient and steady-state flow.

The continuum framework for modelling multiphase subsurface flows assumes that each fluid phase will have its own designated pathway through the pore space, determined by capillary forces, whereby flow of that phase is independent of other fluids present (Armstrong et al., 2016; Blunt, 2017; Dullien, 1992). Thus, the fluid phase interfaces are assumed to be static, and the fluid configurations in equilibrium at the pore scale (Richards, 1931; Leverett, 1941). Changes to this pore scale arrangement to accommodate changes in saturation and pressure are assumed to occur rapidly relative to the macroscopic changes. A quasi-equilibrium state at the pore scale is thus assumed and flow properties are applied indiscriminately to steady and transient flows, as shown in Figure 1 a) in the context of modelling CO_2 plume migration during CO_2 storage. However, even during macroscopically steady-state flow, dynamic fluid interfaces have been observed when the non-wetting phase has a much lower viscosity than the wetting phase, such as CO_2 or natural gas displacing brine. While the average flow properties become invariant in time, there is a continual rearrangement, or intermittency, of fluid flow pathways at the pore scale (Tallakstad, Knudsen, et al., 2009; Armstrong et al., 2016; Rücker et al., 2015; Spurin et al., 2019b, 2019a; Gao et al., 2019; Reynolds et al., 2017; Gao et al., 2020). Static interfaces have been observed between fluids within the pore space during steady-state flow when the non-wetting phase fluid viscosity is similar or higher than that of the wetting phase, such as crude oil displacing brine (Spurin et al., 2019a; Gao et al., 2017; Datta et al., 2014).
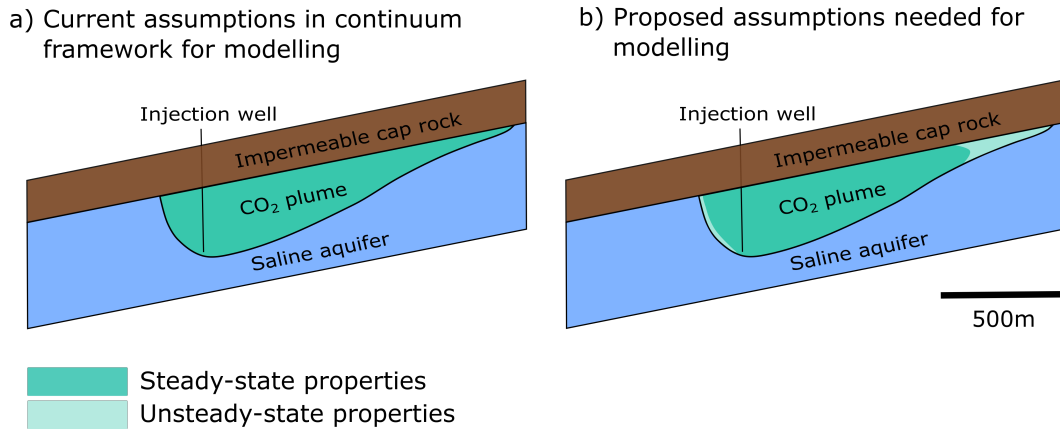
Figure 1. Schematic of the current subsurface modelling framework compared to a potential modelling framework applied here to study CO_2 migration and storage. The CO_2 plume shape was adapted from (MacMinn et al., 2010).

The existence of pore scale intermittency during steady-state flow suggests the possibility of even further complexity during transient flows more typical of the subsurface. This raises the possibility that unsteady-state flows should be modelled with separate upscaled constitutive laws or flow parameters. The transition to steady-state in has been observed in 2D glass micro models as a very rapid evolution after the fluid displacement front has passed (Tallakstad, Løvoll, et al., 2009). However, more complex fluid dynamics are generally observed in rocks (Armstrong et al., 2016; Rücker et al., 2015; Spurin et al., 2019b, 2019a; Gao et al., 2019; Reynolds et al., 2017; Gao et al., 2020). When a non-wetting phase invades a porous rock saturated with the wetting phase, the non-wetting phase travels in rapid, large bursts, referred to as Haines jumps (Haines, 1930; Berg et al., 2013; Bultreys et al., 2015). These rearrangements dissipate large amounts of energy (up to 64% of the input energy (Berg et al., 2013)), and heavily influence unsteady-state flow by altering the mobility of the non-wetting phase. Several theoretical models have been proposed to account for pore scale disequilibrium during transient flows with additional terms in the governing equations (Hassanizadeh et al., 1990; Barenblatt et al., 2003). These models typically introduce flow property dependencies on the rate of change in fluid saturation. However, their applicability, or the development of alternatives, has been limited by the difficulty in making observations at both the small length scales of rock pores and high time resolution of fluid displacement events.

With synchrotron X-ray micro computed tomography, we imaged pore scale fluid dynamics with high time resolution (of 1 second) while macroscopic flow transitioned from transient to steady-state. We aim to establish if the pore scale fluid dynamics underpinning larger scale transient flow are distinguishable from the steady-state dynamics. If distinguishable, transient flows may need to be modelled by distinct flow properties from those of steady-state flows, as demonstrated in Figure 1 b) for CO_2 plume migration during CO_2 storage. To determine if transient flows have distinct flow properties requires observations of the mobility of the fluid phases, and the connectivity of the flow network as the fluid configuration transitions to steady-state. This is explored for a non-wetting phase where intermittency would be expected at macroscopic steady-state (nitrogen) and a non-wetting phase where static interfaces would be expected at steady-state (decane). The non-wetting phase (nitrogen or decane) and the wetting phase (brine) were injected simultaneously into a permeable carbonate rock initially saturated with brine. This is a drainage process as the non-wetting phase initially has to displace brine to percolate across the rock sample. After

Experimental number	Non-wetting phase flow rate (ml/min)	Brine flow rate (ml/min)	Total flow rate (ml/min)	Fractional flow of brine (f_w)	Capillary number
1	0.015 (nitrogen)	0.085	0.1	0.85	1.6×10^{-7}
2	0.03 (nitrogen)	0.07	0.1	0.7	8.7×10^{-8}
3	0.05 (nitrogen)	0.05	0.1	0.5	5.4×10^{-8}
4	0.05 (decane)	0.05	0.1	0.5	2.2×10^{-6}

Table 1. Experimental parameters for the 4 experiments. Calculation of the capillary number is taken from (Spurin et al., 2019a) where $Ca = \frac{q}{\sigma \lambda}$. For a detailed explanation of the experimental procedure, please refer to the Supplementary Material.

this, an equilibrium in the pore scale fluid distribution is reached. To observe the transition to steady-state initiated with two fluid phases already percolating the pore space we also consider two further perturbations inducing unsteady-state for a nitrogen/brine system, by changing the relative flow rate of the fluids.

2 Results

There are four experiments described in this section. These experiments and their parameters are listed in Table 1. In experiment 1 we observed the transition to steady-state from the initial injection of nitrogen into a brine saturated rock. After steady-state had been achieved for experiment 1, and both fluids percolate through the pore space, the system is perturbed twice by changing the flow rate of brine and nitrogen (whilst the total flow rate remains the same); these changes represent experiments 2 and 3. The sample is then re-saturated with brine and the transition to steady-state is observed for decane injected simultaneously with brine; this is experiment 4. We determine macroscopic steady-state primarily through observations of the average pressure gradient across the rock sample, but also verify that average fluid saturation is unchanging.

2.1 Transition to a steady-state with intermittency

The nitrogen and brine were injected simultaneously into a rock saturated with brine (see Table 1 for experimental parameters). The flow was capillary dominated ($Ca = \frac{q}{\sigma \lambda} = 1.6 \times 10^{-7}$ where q is the total Darcy flux, σ the interfacial tension between the non-wetting phase (nw) and brine, and λ the mobility) and the mobility ($\lambda = \frac{f_w}{\mu_{brine}} + \frac{1-f_w}{\mu_{nw}}$ where μ is the viscosity and f_w is the brine flow rate as a fraction of the total flow rate) indicated that intermittency was expected at steady-state (Spurin et al., 2019a). Macroscopic steady-state was determined based on the differential pressure across the rock sample (Figure 2). The pressure differential increased with the initial invasion of the non-wetting phase. It then continued to increase after the non-wetting phase had percolated across the rock, before finally plateauing and oscillating around a constant mean value with a period of approximately 10 minutes, which was considered steady-state.

Prior to percolation, the pressure increased monotonically (labels 1 and 2 in Figure 2) and there were large changes in gas saturation as gas was establishing a percolating path through the pore space. This did not induce major changes in the number of disconnected gas regions (ganglia), shown in Figure 3. The gas propagated in large bursts (Haines jumps (Haines, 1930; Berg et al., 2013; Bultreys et al., 2015)) that incorporated a large number of connected pores (Figure 4).
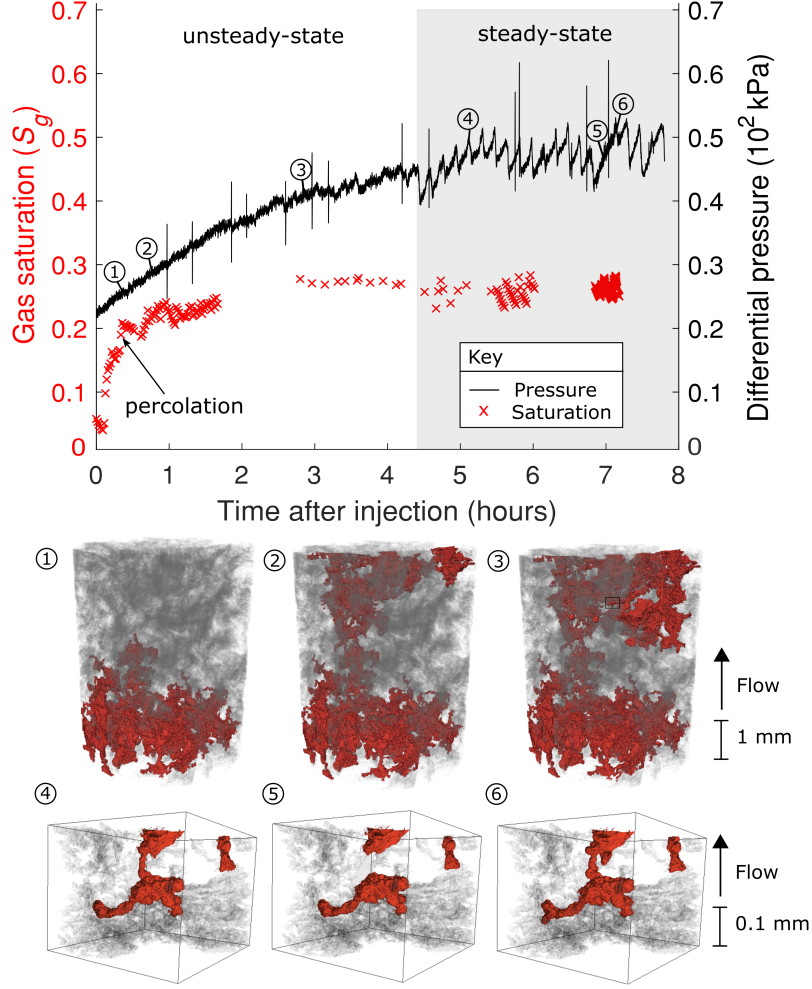
Figure 2. Top: the gas saturation and differential pressure time series following the initial perturbation (experiment 1 in Table 1). Bottom: images of the pore space at the indicated times in experiment 1. The gas is red, the brine is grey and the rock grains are transparent. The first three images are for the entire imaged section of the rock. At steady-state the dynamics are more subtle and so the final three images are zoomed in on a smaller region of the pore space indicated by a square in panel 3 See the supplementary information for videos of the dynamics.
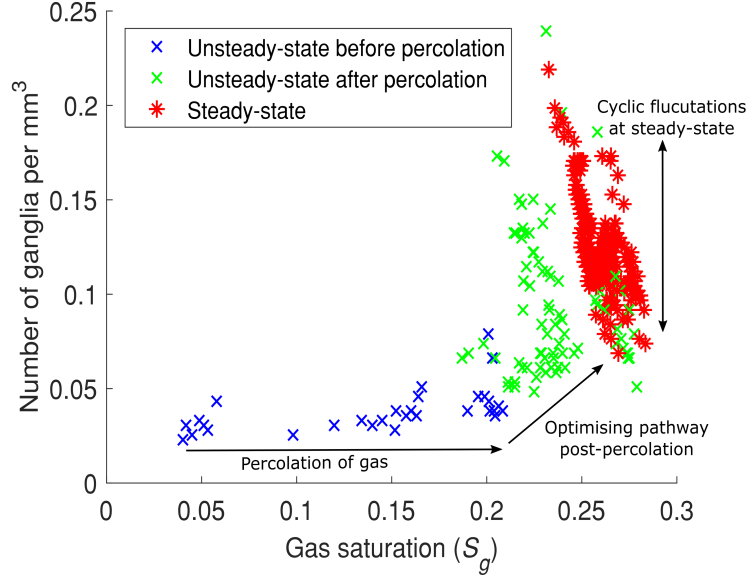
Figure 3. The gas saturation against the number of disconnected gas regions for experiment 1 - see Table 1 and Figure 2. At steady-state, there are many disconnection and reconnection events (intermittent pathway flow) resulting in a wide range in the connectivity in the gas, however, the saturation fluctuates over a much smaller range.
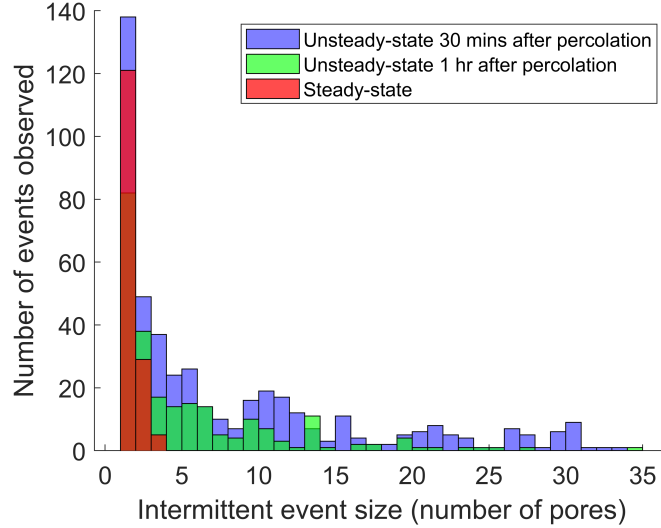

Figure 4. The size of an intermittently occupied part of the pore space decreases as we approach steady-state from the initial invasion (experiment 1 see Table 1 and Figures 2 and 3). The number of intermittent events also deceases.

After percolation but prior to steady-state, the gas saturation increased, but less rapidly than before percolation, and the number of disconnected gas regions increased as the pathway through the pore space was optimised (Figure 3). This change in flow behaviour corresponded to a decrease in the rate of change of the pressure differential in Figure 2. During the transition to steady-state, the average number of pores involved in an intermittent event decreased from greater than 30 pores to less than 5 (Figure 4). The total number of intermittent events also decreased (Figure 4). The number and size of intermittent events decreased as the gas found the optimal pathway through the system, but some flow pathways remained intermittent despite the flow being macroscopically steady-state flow, as shown by the pressure differential data (Figure 2).

At steady-state, the gas saturation plateaued and oscillated around an average value of $S_g = 0.26 \pm 0.02$, with a cycle lasting approximately 10 minutes in Figure 2; there was no net change in saturation when averaging over a differential pressure cycle. The number of disconnected gas regions fluctuated significantly (the range was $\pm$ 70% of the mean) at steady-state, but the fluctuation in the saturation was much smaller (the range was $\pm$ 15% of the mean) (Figure 3). The size of the intermittent events was significantly lower than during the transition, generally involving only a single pore (Figures 4 and 2). This means that small changes at critical locations in the pore space led to major changes in the connectivity of the gas, demonstrated by the disconnecting and reconnecting of a region of gas from the main flow pathway by one periodic pathway that encompasses only one pore in panels 4-6 in Figure 2.

2.2 Transition to steady-state after a perturbation

The system was perturbed twice by changing the relative flow rates of the fluids while maintaining the total flow rate of gas and brine (experiments 2 and 3 in Table 1). A flow pathway had been established from the initial percolation (experiment 1), but by increasing the gas flow rate, the capillary pressure was increased and the gas was able to enter previously inaccessible pores. With this perturbation, the changes in system properties - pressure, saturation, intermittency - were more subtle than with the initial percolation (Figure 5).

Figure 6 shows that the majority of the pore space was continuously occupied by either brine or gas (less than 2% of the pore space was occupied intermittently by both phases). However, the impact of these intermittent flow pathways on the connectivity of the gas was significant, as shown in Figure 3. The peak for the amount of intermittent pathway flow during steady-state was observed when the brine flow rate constituted 70% of the total flow rate (experiment 2 in Figure 6, with details in Table 1). This agrees with previous observations of intermittency during steady-state flow (Spurin et al., 2019b). We therefore observed the transition to a state with more intermittent pathway flow (from experiment 1 to experiment 2) and, subsequently, the transition to a state with less intermittent pathway flow (from experiment 2 to experiment 3).

When transitioning to steady-state for experiment 2, where the steady-state intermittency is more than the previous step, we observe a gradual increase in gas saturation and intermittency (Figures 5 and 6, respectively). This makes this transition markedly different from the initial percolation (experiment 1), where the dynamics were largest at the onset, and then reduced to small movements (Figure 4). Many of the flow pathways were established during the initial percolation phase and so the transition to steady-state was quicker. The modest increase in intermittency is associated with the opening of new pathways to accommodate the greater gas flux. The long period (approximately 10 minute) pressure differential oscillations persist through the perturbation (Figure 5).

When transitioning to steady-state for experiment 3, where the steady-state intermittency is less than the previous step, we observe an increase in gas saturation and a gradual decrease in intermittency (Figures 5 and 6, respectively). The transition to steady-state is quickest for this experiment (Figure 5).
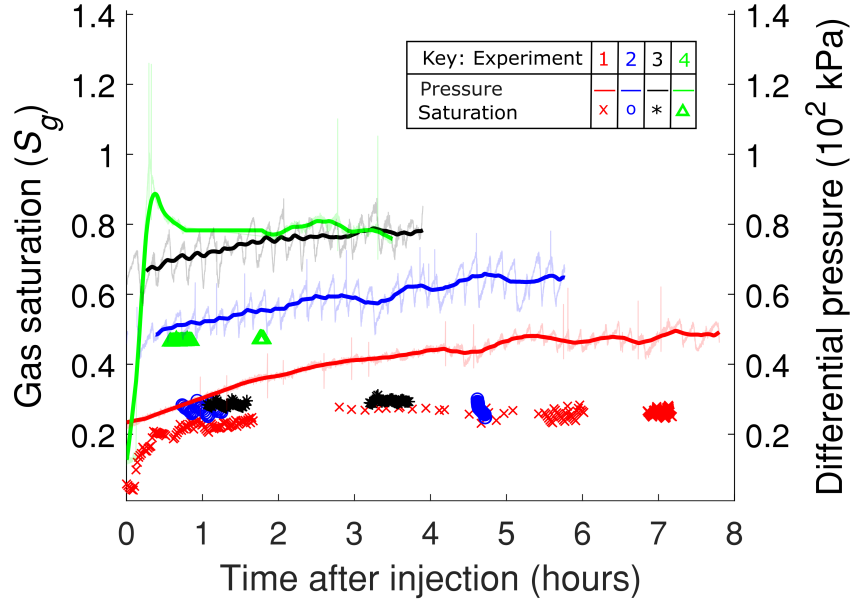
Figure 5. The gas saturation and differential pressure as a function of time. The raw pressure data is shown in light colouring while the bold colouring shows the pressure data averaged over a period of an oscillation to clearly show the transition to steady-state. See Table 1 for the experimental parameters.
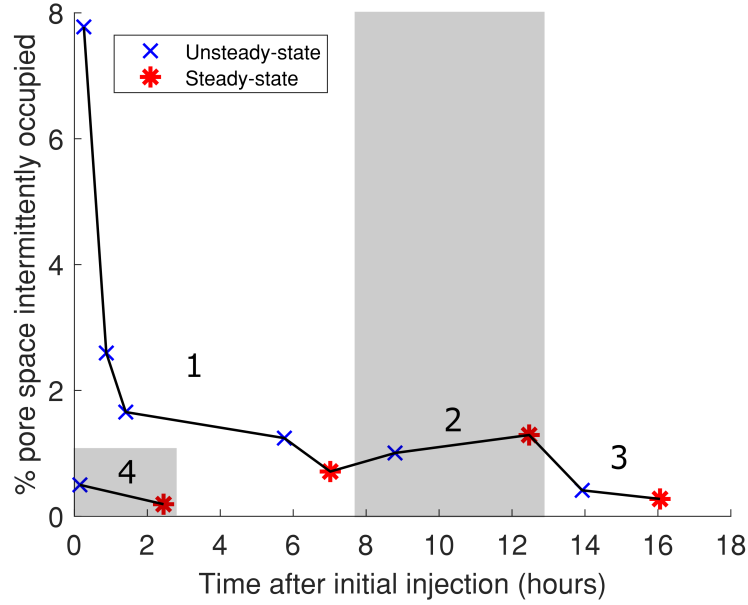

Figure 6. The percentage volume of the pore space identified as intermittent. Each point is the average of 10 minute window of continuous imaging. The different experiments (as listed in Table 1) are labelled on the image.
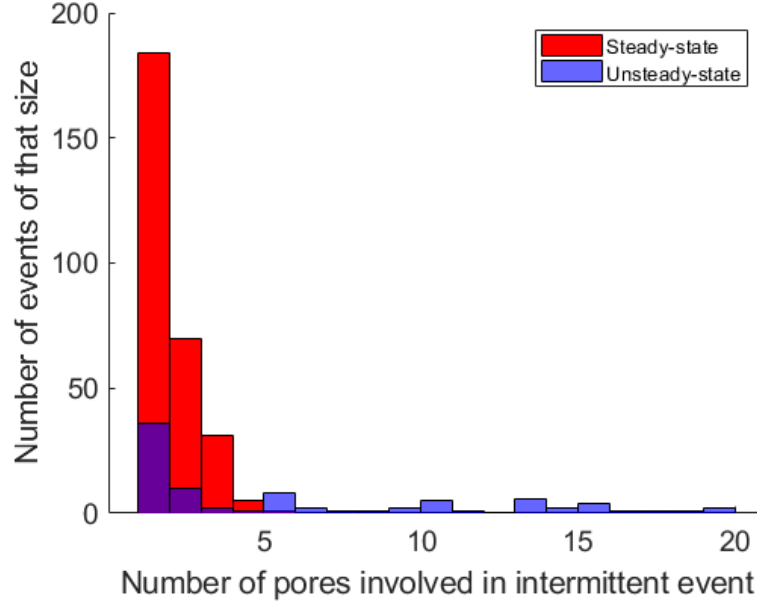
Figure 7. The size of an intermittently occupied part of the pore space decreases as we approach steady-state for experiment 2, where a perturbation was initiated in a steady state percolating system by changing the relative flow rates of nitrogen and brine. Figure 4 is the equivalent figure but for experiment 1. Similar evolutions are observed for experiments 3 and 4.

Overall, transitions to steady state after an initial percolation had occurred are characterised by gradual changes in intermittency between an initial and final saturation state regardless of whether the intermittency is increasing or decreasing. However, even with little change in saturation the size of intermittent events is much larger during the transient than steady-state flow, similar to observations made during the initial percolation (Figure 7). It is thus a general feature of flow during both the initial percolation and subsequent perturbations that unsteady-state movements incorporate larger events (up to 20 pores involved in an intermittent event) whereas steady-state pathways involve much smaller events (always less than 5 pores) (Figure 7).

2.3 Transition to a steady-state with no intermittency

The sample was re-saturated with brine and an experiment was conducted with decane as the non-wetting phase to explore the role of viscosity on the transition to steady-state (experiment 4 in Table 1). The viscosity ratio has been identified as a primary variable controlling intermittency, with less dynamics expected at steady-state for systems with more viscous non-wetting fluids (Spurin et al., 2019b). The flow rate was matched with the gas experiments and the capillary number is higher by an order of magnitude due to the viscosity of the oil (although flow is still capillary dominated, Table 1).

The initial transition to steady-state was much quicker (taking less than an hour) than with gas, shown in Figures 5 and 6. The oil saturation is higher than the gas saturation in experiment 3 as expected from increasing the non-wetting phase viscosity (Figure 5). The fluctuations in pressure are much smaller than for the gas experiments. We do observe intermittency during the transition to steady-state. However, it is far less prevalent than during the initial nitrogen percolation (Figure 6) and it evolves more quickly (Figure 5).

As expected, there is almost no intermittency at steady-state (0.2% of the pore space is identified as intermittent).

3 Conclusions

Intermittent fluid flow pathways were always observed during macroscopically transient flow. These intermittent flow pathways constituted a larger volume of the pore space and were most frequent after the initial invasion of the fluids and were distinct from steady-state intermittent pathways by size and frequency.

The mobility of the non-wetting phase was observed to be different during transient flow. The change in saturation after percolation was small (the saturation was already 88% of the steady-sate saturation at the time of percolation), but there was a much larger increase in pressure (the differential pressure was 70% of the steady-state differential pressure at percolation). This means that the change in saturation per unit time is smaller than the change in the total mobility of the fluids per unit time (which is inversely proportional to the pressure drop). The mobility of the non-wetting phase, for a given saturation, is higher for a lower differential pressure. This implies that the non-wetting phase was more mobile in the transitional stage than at steady-state and that intermittency is associated with higher mobility of the non-wetting fluid phase. These results suggest that transient flow dynamics should not be modelled using steady-state flow properties. However, current models that do consider dynamic effects suggest these effects may be parameterised by rates of change of fluid saturation (Barenblatt et al., 2003; Hassanizadeh et al., 2002). This approach cannot be applied to our experiments because the saturation remains approximately constant while the total mobility changes significantly.

We estimate the length scale in the fluid plume front from which steady-state dynamics can be assumed and applied to scenarios, such as in Figure 1 b). Steady-state was achieved after the initial invasion in experiment 1 after approximately 180 pore volumes of gas were injected through a sample 20 mm in length. This would correspond to a plume front governed by transient flow dynamics approximately 3.6 m thick. For experiment 4, steady-state was achieved after approximately 60 pore volumes of gas were injected, corresponding to a distance of approximately 0.9 m. This means the transition zone would be much smaller for systems such as conventional and heavy oil, and NAPL contamination, where intermittency is not expected at subsurface flow conditions.

There are added complexities in subsurface applications if the injected phase is already present, or if the plume is layered due to geological constraints. Firstly, if the non-wetting phase is already present, then the transition to steady-state is less evident than it was for the initial invasion of gas. Changing the flow parameters once the non-wetting phase had percolated the pore space resulted in gradual changes in saturation and intermittency as a new steady-state was established. Secondly, for the Sleipner CO_2 plume, as an example, the plume exists as layers that are frequently 1-5 m thick (R. Chadwick et al., 2009). Our work suggests that the leading edge of the CO_2 plume in the unsteady-state regime is indeed more mobile than would be predicted by current quasi-steady-state models. This effect would be more noticeable in a layered plume with multiple plume fronts. These complexities may provide an explanation to why predictive modelling subsurface fluid flows at field relevant scales (100 - 1000m) is notoriously difficult, exemplified by the many attempts to model CO_2 plume migration in a saline aquifer at Sleipner (Williams & Chadwick, 2017; Singh et al., 2010; R. A. Chadwick & Noy, 2015; Zhu et al., 2015; Cavanagh & Haszeldine, 2014). Existing models that include transient dynamics focus on the rate dependence of saturation or capillary pressure, which do not necessarily change significantly in this transition (Barenblatt et al., 2003; Hassanizadeh et al., 2002, 1990; Picchi & Battiato, 2018). Hence, we suggest that a new modelling framework should be explored to account for the behaviour we have observed.

4 Materials and Methods

The experiments were conducted in a cylindrical Estaillades sample, 5 mm diameter and 20 mm length. The sample was attached to a dual injection piece, specifically designed for the simultaneous injection of two fluid phases while suppressing the generation of slug flow. The sample was initially saturated with brine (deionised water doped with 15% wt. KI to improve the X-ray contrast). The system was pressurised to 8 MPa to minimise the compressibility of nitrogen, with an additional 2 MPa of confining pressure. Then both nitrogen and brine were injected simultaneously, with the flow rates of the nitrogen and the brine listed in Table 1. A differential pressure transducer (Keller, 300 kPa transducer with 1.5 kPa accuracy) was connected across the sample, to measure the pressure drop. Steady-state was determined to be reached once the differential pressure had plateaued. The sample was resaturated with brine at the end of the nitrogen experiments, and the experiment was repeated with decane and brine injected simultaneously.

The X-ray imaging was conducted at the TOMCAT beamline at the Swiss Light Source, Paul Scherrer Institut, Villigen, Switzerland. The sample was exposed to filtered polychromatic X-ray radiation with a peak energy of about 26 keV originating from a 2.9 T bending magnet source. The filter was 2300 μm-thick Silicon. An in-house developed GigaFRoST camera (Mokso et al., 2017) and a high numerical aperture white-beam microscope (Optique Peter) with 4x magnification (Bührer et al., 2019) were used, yielding an effective pixel size of 2.75 μm. Each tomogram contained 1000 projections over 180° rotation. Each scan lasted 1 s, with a further 1 s required for the sample to rotate back to its initial position before the next scan could begin.

Each image analysed was 4224 × 4298 × 4263 μm in size. The images were reconstructed from the X-ray projections using the propagation-based phase contrast method (Paganin et al., 2002) and the gridrec algorithm (Marone & Stampanoni, 2012). The images were then filtered with a non-local means filter to suppress noise whilst maintaining the information at phase boundaries (Schlüter et al., 2014). The first image was taken with just deionised water in the pore space. This image is used to segment the pore space from the rock grains using a watershed segmentation algorithm (Beucher & Meyer, 1993). Then the sample was saturated with the brine, and another image was taken; this is the brine saturated imaged. All subsequent images with the non-wetting phase (nitrogen or decane) and brine present were subtracted from the brine saturated image, this results in a differential image whereby only the location of non-wetting phase remains. From this a simple greyscale value threshold can be used to segment out the nitrogen. The pore space was overlain on this segmentation to locate the pore space occupied with brine.

The pore space morphology was extracted using a maximal inscribed spheres (maximum ball, MB) network extraction technique (Dong & Blunt, 2009; Raeini et al., 2017). The fluid occupancy for each pore MB was assigned for every time step. Then for every pore, the neighbouring pores are listed with their occupancy. Using this, the size of an intermittent can be calculate, resulting in Figures 4 and 7.

References

Armstrong, R. T., McClure, J. E., Berrill, M. A., Rücker, M., Schlüter, S., & Berg, S. (2016). Beyond Darcy's law: The role of phase topology and ganglion dynamics for two-fluid flow. *Physical Review E*, *94*(4), 043113.

Bachu, S. (2000). Sequestration of CO_2 in geological media: criteria and approach for site selection in response to climate change. *Energy Conversion and Management*, *41*(9), 953–970.

Barenblatt, G., Patzek, T. W., & Silin, D. (2003). The mathematical model of nonequilibrium effects in water-oil displacement. *SPE journal*, *8*(04), 409–416.

Berg, S., Ott, H., Klapp, S. A., Schwing, A., Neiteler, R., Brussee, N., . . . others (2013).

Real-time 3D imaging of haines jumps in porous media flow. *Proceedings of the National Academy of Sciences*, *110*(10), 3755–3759.

Beucher, S., & Meyer, F. (1993). The morphological approach to segmentation: the watershed transformation. *Mathematical morphology in image processing*, *34*, 433–481.

Bickle, M. J. (2009). Geological carbon storage. *Nature Geoscience*, *2*(12), 815–818.

Blunt, M. J. (2017). *Multiphase flow in permeable media: A pore-scale perspective*. Cambridge University Press.

Bührer, M., Stampanoni, M., Rochet, X., Büchi, F., Eller, J., & Marone, F. (2019). High-numerical-aperture macroscope optics for time-resolved experiments. *Journal of synchrotron radiation*, *26*(4).

Bultreys, T., Boone, M. A., Boone, M. N., De Schryver, T., Masschaele, B., Van Loo, D., ... Cnudde, V. (2015). Real-time visualization of Haines jumps in sandstone with laboratory-based microcomputed tomography. *Water Resources Research*, *51*(10), 8668–8676.

Cavanagh, A. J., & Haszeldine, R. S. (2014). The Sleipner storage site: Capillary flow modeling of a layered CO_2 plume requires fractured shale barriers within the Utsira Formation. *International Journal of Greenhouse Gas Control*, *21*, 101–112.

Chadwick, R., Noy, D., Arts, R., & Eiken, O. (2009). Latest time-lapse seismic data from Sleipner yield new insights into CO_2 plume development. *Energy Procedia*, *1*(1), 2103–2110.

Chadwick, R. A., & Noy, D. J. (2015). Underground CO_2 storage: demonstrating regulatory conformance by convergence of history-matched modeled and observed CO_2 plume behavior using Sleipner time-lapse seismics. *Greenhouse Gases: Science and Technology*, *5*(3), 305–322.

Datta, S. S., Ramakrishnan, T., & Weitz, D. A. (2014). Mobilization of a trapped non-wetting fluid from a three-dimensional porous medium. *Physics of Fluids*, *26*(2), 022002.

Dong, H., & Blunt, M. J. (2009). Pore-network extraction from micro-computerized-tomography images. *Physical Review E*, *80*(3), 036307.

Dullien, F. A. (1992). *Porous media: fluid transport and pore structure*. Academic Press.

Gao, Y., Lin, Q., Bijeljic, B., & Blunt, M. J. (2017). X-ray microtomography of intermittency in multiphase flow at steady state using a differential imaging method. *Water Resources Research*, *53*(12), 10274–10292.

Gao, Y., Lin, Q., Bijeljic, B., & Blunt, M. J. (2020). Pore-scale dynamics and the multiphase darcy law. *Physical Review Fluids*, *5*(1), 013801.

Gao, Y., Raeini, A. Q., Blunt, M. J., & Bijeljic, B. (2019). Pore occupancy, relative permeability and flow intermittency measurements using X-ray micro-tomography in a complex carbonate. *Advances in Water Resources*, *129*, 56–69.

Haines, W. B. (1930). Studies in the physical properties of soil. v. the hysteresis effect in capillary properties, and the modes of moisture distribution associated therewith. *The Journal of Agricultural Science*, *20*(1), 97–116.

Hassanizadeh, S. M., Celia, M. A., & Dahle, H. K. (2002). Dynamic effect in the capillary pressure–saturation relationship and its impacts on unsaturated flow. *Vadose Zone Journal*, *1*(1), 38–57.

Hassanizadeh, S. M., Gray, W. G., et al. (1990). Mechanics and thermodynamics of multiphase flow in porous media including interphase boundaries. *Adv. Water Resour*, *13*(4), 169–186.

Leverett, M. (1941). Capillary behavior in porous solids. *Transactions of the AIME*, *142*(01), 152–169.

MacMinn, C. W., Szulczewski, M. L., & Juanes, R. (2010). CO_2 migration in saline aquifers. Part 1. capillary trapping under slope and groundwater flow. *Journal of Fluid Mechanics*, *662*, 329–351.

Marone, F., & Stampanoni, M. (2012). Regridding reconstruction algorithm for real-time tomographic imaging. *Journal of synchrotron radiation*, *19*(6), 1029–1037.

Mokso, R., Schlepütz, C. M., Theidel, G., Billich, H., Schmid, E., Celcer, T., ... oth-

ers (2017). Gigafrost: the gigabit fast readout system for tomography. *Journal of synchrotron radiation*, *24*(6), 1250–1259.

Paganin, D., Mayo, S. C., Gureyev, T. E., Miller, P. R., & Wilkins, S. W. (2002). Simultaneous phase and amplitude extraction from a single defocused image of a homogeneous object. *Journal of microscopy*, *206*(1), 33–40.

Picchi, D., & Battiato, I. (2018). The impact of pore-scale flow regimes on upscaling of immiscible two-phase flow in porous media. *Water Resources Research*, *54*(9), 6683–6707.

Pye, V. I., & Patrick, R. (1983). Ground water contamination in the United States. *Science*, *221*(4612), 713–718.

Raeini, A. Q., Bijeljic, B., & Blunt, M. J. (2017). Generalized network modeling: Network extraction as a coarse-scale discretization of the void space of porous media. *Physical Review E*, *96*(1), 013312.

Reynolds, C. A., Menke, H., Andrew, M., Blunt, M. J., & Krevor, S. (2017). Dynamic fluid connectivity during steady-state multiphase flow in a sandstone. *Proceedings of the National Academy of Sciences*, *114*(31), 8187–8192.

Richards, L. A. (1931). Capillary conduction of liquids through porous mediums. *Physics*, *1*(5), 318–333.

Rubin, E., & De Coninck, H. (2005). IPCC special report on carbon dioxide capture and storage. *UK: Cambridge University Press. TNO (2004): Cost Curves for CO2 Storage, Part*, *2*, 14.

Rücker, M., Berg, S., Armstrong, R., Georgiadis, A., Ott, H., Schwing, A., ... others (2015). From connected pathway flow to ganglion dynamics. *Geophysical Research Letters*, *42*(10), 3888–3894.

Schlüter, S., Sheppard, A., Brown, K., & Wildenschild, D. (2014). Image processing of multiphase images obtained via X-ray microtomography: a review. *Water Resources Research*, *50*(4), 3615–3639.

Singh, V. P., Cavanagh, A., Hansen, H., Nazarian, B., Iding, M., & Ringrose, P. S. (2010). Reservoir modeling of CO_2 plume behavior calibrated against monitoring data from Sleipner, Norway. In *Spe annual technical conference and exhibition* (Vol. 134891).

Spurin, C., Bultreys, T., Bijeljic, B., Blunt, M. J., & Krevor, S. (2019a). Mechanisms controlling fluid break-up and reconnection during two-phase flow in porous media. *Physical Review E*, *100*(4), 043115.

Spurin, C., Bultreys, T., Bijeljic, B., Blunt, M. J., & Krevor, S. (2019b). Intermittent fluid connectivity during two-phase flow in a heterogeneous carbonate rock. *Physical Review E*, *100*(4), 043103.

Tallakstad, K. T., Knudsen, H. A., Ramstad, T., Løvoll, G., Måløy, K. J., Toussaint, R., & Flekkøy, E. G. (2009). Steady-state two-phase flow in porous media: statistics and transport properties. *Physical Review Letters*, *102*(7), 074502.

Tallakstad, K. T., Løvoll, G., Knudsen, H. A., Ramstad, T., Flekkøy, E. G., & Måløy, K. J. (2009). Steady-state, simultaneous two-phase flow in porous media: An experimental study. *Physical Review E*, *80*(3), 036308.

Williams, G. A., & Chadwick, R. A. (2017). An improved history-match for layer spreading within the Sleipner plume including thermal propagation effects. *Energy Procedia*, *114*, 2856–2870.

Zhu, C., Zhang, G., Lu, P., Meng, L., & Ji, X. (2015). Benchmark modeling of the Sleipner CO_2 plume: Calibration to seismic data for the uppermost layer and model sensitivity analysis. *International Journal of Greenhouse Gas Control*, *43*, 233–246.

Acknowledgments